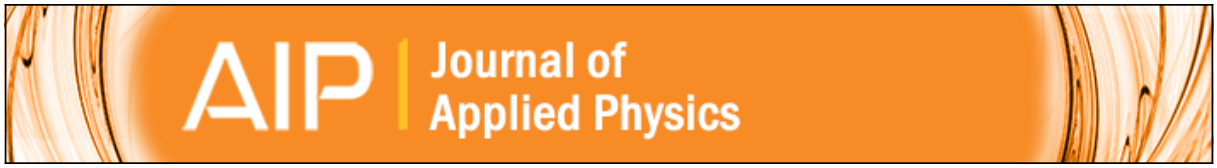

Charge transport in highly efficient iridium cored electrophosphorescent dendrimers

Jonathan P. J. Markham, Ifor D. W. Samuel, Shih-Chun Lo, Paul L. Burn, Martin Weiter, and Heinz Bässler

Citation: Journal of Applied Physics **95**, 438 (2004); doi: 10.1063/1.1633336

View online: http://dx.doi.org/10.1063/1.1633336

View Table of Contents: http://scitation.aip.org/content/aip/journal/jap/95/2?ver=pdfcov

Published by the AIP Publishing

Charge transport in highly efficient iridium cored electrophosphorescent dendrimers

Jonathan P. J. Markham and Ifor D. W. Samuel[a)]
Organic Semiconductor Center, School of Physics and Astronomy, University of St Andrews, North Haugh, St Andrews, Fife, KY16 9SS, United Kingdom

Shih-Chun Lo and Paul L. Burn[b)]
The Dyson Perrins Laboratory, Oxford University, South Parks Road, Oxford, OX1 3QY, United Kingdom

Martin Weiter and Heinz Bässler
Institute of Physical, Nuclear and Macromolecular Chemistry and Material Science Center, Philipps-Universität Marburg, Hans-Meerwein-Strasse, D-35032 Marburg, Germany

(Received 5 August 2003; accepted 23 October 2003)

Electrophosphorescent dendrimers are promising materials for highly efficient light-emitting diodes. They consist of a phosphorescent core onto which dendritic groups are attached. Here, we present an investigation into the optical and electronic properties of highly efficient phosphorescent dendrimers. The effect of dendrimer structure on charge transport and optical properties is studied using temperature-dependent charge-generation-layer time-of-flight measurements and current voltage ($I-V$) analysis. A model is used to explain trends seen in the $I-V$ characteristics. We demonstrate that fine tuning the mobility by chemical structure is possible in these dendrimers and show that this can lead to highly efficient bilayer dendrimer light-emitting diodes with neat emissive layers. Power efficiencies of 20 lm/W were measured for devices containing a second-generation (G2) $Ir(ppy)_3$ dendrimer with a 1,3,5-tris(2-N-phenylbenzimidazolyl)benzene electron transport layer. © *2004 American Institute of Physics.* [DOI: 10.1063/1.1633336]

I. INTRODUCTION

Since early reports of organic electroluminescence (EL) in small molecules,[1] polymers,[2] and conjugated dendrimers,[3,4] dramatic improvements in the efficiency and stability of these materials have been achieved. Now, external quantum efficiencies (EQEs) of organic light-emitting diodes (OLEDs) are of the order of 10%–20%[5] and lifetimes in excess of 10 000 h (Ref. 6) have been reported. In particular, the development of electrophosphorescent devices[7] has allowed triplet harvesting and the production of highly efficient devices. In this area, iridium-based phosphors have received much attention due to their highly efficient phosphorescence, color tunability, and relatively short excited state lifetime. Both evaporated[8] and solution processed[9] devices have been reported. Our approach to solution processing of phosphorescent materials is to use conjugated dendrimers and we have developed highly efficient single and bilayer devices using this method.[10,11]

Time of flight (TOF) mobility measurements are a powerful technique for the investigation of charge transport in organic materials. However, they have not yet been applied to electrophosphorescent materials. Here, we apply the technique in the context of electrophosphorescent dendrimers, which give us scope for the tuning of properties, such as interchromophore spacing and thus the mobility. An important feature of this work is the use of the charge-generation-layer time-of-flight (CGL-TOF) method (explained in Sec. II). For the conventional, bulk-excitation TOF method, a very thick (μm dimensions) film is usually necessary. For solution processable materials, this often entails the production of a drop cast film. Two problems arise in using this latter technique. One is that the morphology of the sample may be very different from that produced by spin coating, and mobility in organic materials has been shown to be heavily dependent upon the film morphology. The second is that the mobility is measured upon a sample that is of much greater thickness than that used for OLEDs. In many cases of dispersive transport, a thickness dependence of the mobility is observed and this may call into question the relevance of such measurements to light-emitting device (LED) design. In the present work, we overcome both these problems by utilizing a spin-coated layer of ~400 nm thickness and a charge-generation layer of absorptive dye. This enables a well-defined charge generation point even in a thin sample. It therefore allows the study of much thinner samples that can be produced by spin casting with morphological properties of direct relevance to LED structures. We have recently reported measurements of nondispersive hole transport in a fluorescent blue-emitting dendrimer film using the above technique.[12]

Conjugated dendrimers consist of a light-emitting core, dendrons, and surface groups. One of the great advantages of this molecular framework is that each of the components can be tuned independently to control the color of emission, degree of intermolecular interaction, and solubility as required for different applications. Dendrimers can be synthesized in

a)Electronic mail: idws@st-and.ac.uk
b)Electronic mail: paul.burn@chem.ox.ac.uk

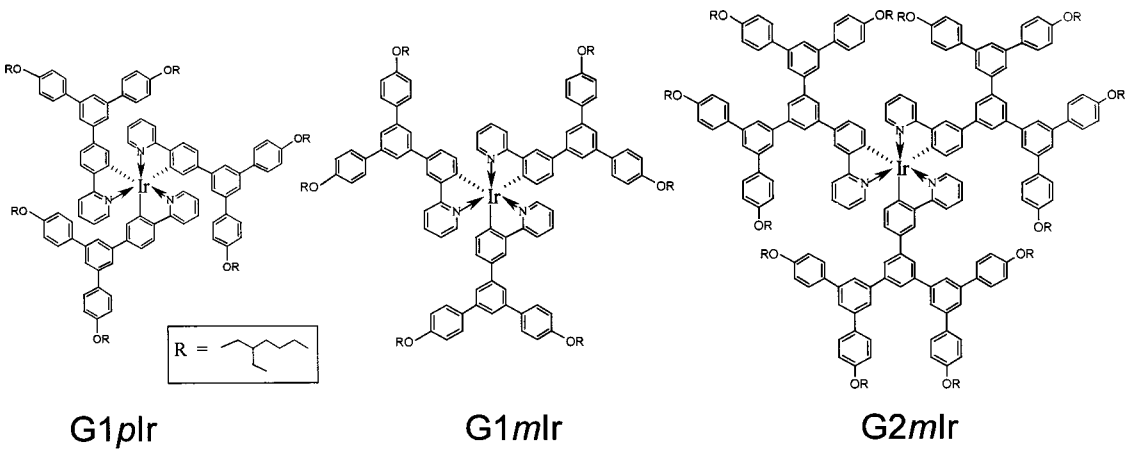

FIG. 1. Structures of the three iridium dendrimers (from the left-hand side) G1*p*Ir, G1*m*Ir, and G2*m*Ir.

an orderly manner such that the macromolecules are monodisperse and the structure is precisely known. Thus, there is little issue of batch to batch reproducibility. It has already been shown that a dendrimer consisting of a fluorescent core and wide band-gap dendrons behaves very much like a molecularly doped polymer albeit with a much more regulated and accurately controlled interchromophore separation.[13]

Charge transport has been studied widely in solution-processible conjugated polymers. It is known for these systems that different solvents and spinning conditions can produce very different thin-film morphologies. In addition, even in relatively ordered materials, such as ladder-type polymers, sample history has been shown to have a dramatic effect on the measured charge transport and optical properties.[14] This may partly explain the wide range of mobilities measured for some of these materials.[15] The mobility of carriers along polymer chains can be quite high[16] and, in these cases, the rate-limiting step is the degree of disorder in the material. This makes the optimization of the mobility within a neat organic layer relatively challenging for most spin-coated materials. However, in contrast, dendrimers allow the precise control of the core separation. In this article, we demonstrate that by altering the generation number (or level of branching) and attachment point of the dendron to the core we are able to fine tune the hole mobility and optical properties of these highly efficient iridium-based dendrimers.

II. EXPERIMENT

The dendrimers studied here are based on a *fac*-tris(2-phenylpyridyl) iridium (III) [$Ir(ppy)_3$] core, phenylene dendrons and 2-ethylhexyloxy surface groups. They are: G1-*meta*-$Ir(ppy)_3$ (hence referred to as G1*m*Ir), G1-*para*-$Ir(ppy)_3$ (G1*p*Ir), and G2-*meta*-$Ir(ppy)_3$ (G2*m*Ir). Their structures are shown in Fig. 1. All are soluble in organic solvents, such as tetrahydrofuran, toluene, and chloroform. G1*m*Ir has been previously used to give very high efficiency solution processed OLEDs.[10,11]

CGL-TOF measurements were performed on 300–400 nm thick dendrimer films spin coated onto cleaned indium-tin oxide (ITO) substrates (sheet resistance 20 Ω/□) from 40 mg/ml chloroform solutions of dendrimer. Subsequently, 10 nm of perylene diimide charge-generation layer was evaporated onto the device covering the whole substrate. The device was completed by deposition of 100 nm of aluminum to give an active pixel area of approximately 5 mm^2. The excitation wavelength was chosen to pass through the bulk film under study and to be absorbed by the perylene dye. Charge carriers were generated within the perylene layer by excitation from a 10 ns pulse of a frequency-doubled Nd:Yttrium aluminum garnet laser at a wavelength of 532 nm. The packet of charge carriers was then swept through the device under an applied field, and the time for the packet to travel across the device, known as the transit time (t_{tr}) was measured. The aluminum electrode was biased positively and the photocurrent signal detected from the ITO using the 50 Ω input of a digital storage oscilloscope. The applied bias led to the electrons photogenerated in the perylene diimide layer being removed from the diode at the aluminum electrode and holes being injected into the dendrimer from the perylene dye and consequently swept across the device to be annihilated at the ITO electrode. Thus, the measured photocurrent transients correspond to hole currents.

Single and bilayer LEDs were fabricated on solution etched ITO substrates. The ITO was cleaned in ultrasonic baths of acetone and 2-propanol, before oxygen plasma ashing under a pressure of 10^{-2} mbar at 100 W for 5 min (Emitech Model K-1050X). Dendrimer films were spin coated from 20 mg/ml chloroform solutions to give film thicknesses of 120 nm for single layer devices and 80 nm for bilayer devices. Cathode evaporation of 20 nm of calcium capped with 100 nm of aluminum completed the single layer devices. Bilayer devices were fabricated by evaporation of 50 nm of 1,3,5-tris(2-*N*-phenylbenzimidazolyl)benzene (TPBI) as an electron transporting/hole blocking layer and a cathode of 1 nm LiF capped with 100 nm aluminum completed the device. In both cases, the pixel area was approximately 8 mm^2.

All EL measurements were performed under a vacuum using a Keithley 2400 source measure unit and calibrated photodiode. Efficiency calculations were performed by measuring the light output in the forward direction[17] and bright-

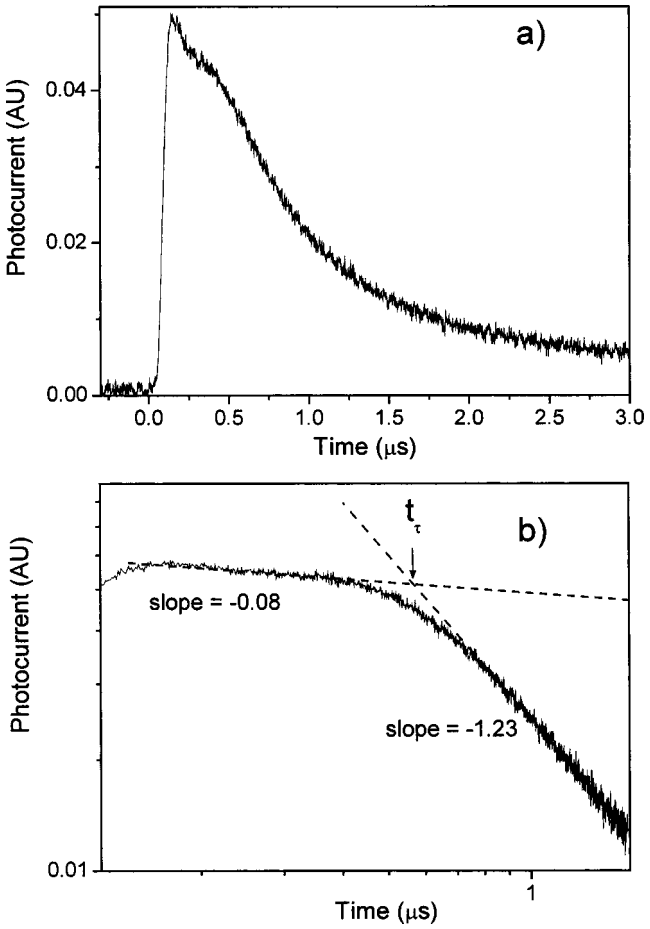

FIG. 2. (a) G1*m*Ir transient photocurrent at 298 K and field of 1.2×10^6 V/cm. (b) The same transient photocurrent plotted in a double logarithmic form.

ness measurements were cross checked with a Minolta LS-100 luminance meter.

III. RESULTS AND DISCUSSION

A. Mobility measurements

The CGL-TOF method was used to measure the mobilities of G1*p*Ir, G1*m*Ir, and G2*m*Ir iridium cored dendrimers shown in Fig. 1. A typical transient for a G1*m*Ir film of 330 nm thickness at room temperature and an applied field of 1.2×10^6 V/cm is shown in Fig. 2(a). It can be seen that the transient is weakly dispersive. After the initial photocurrent peak, there is a long photocurrent tail. The shoulder is close to the photocurrent peak because the sample is much thinner than the micron thicknesses usually used in TOF. The mobility can be calculated from the intersection of the asymptotes to the two power-law regions of the transients [Fig. 2(b)]. Using Eq. (1), we calculate a mobility of 4.5×10^{-5} $\mathrm{cm}^2/\mathrm{V\,s}$

$$\mu=\frac{d^2}{Vt_{\mathrm{tr}}}. \tag{1}$$

Here μ is the mobility, d the device thickness, V the applied voltage and t_{tr} the transit time.

The transients shown here are weakly dispersive at room temperature, however an attempt to analyze them in terms of the Scher–Montroll[18] theory was not successful. When plotted on a double logarithmic scale, this theory relates the two power-law regions of the transient before and after the transit time by a disorder parameter α, as seen in Eq. (2)

$$I(t)\sim t^{-(1-\alpha)} \quad (t<t_{\mathrm{tr}})$$
$$I(t)\sim t^{-(1+\alpha)} \quad (t>t_{\mathrm{tr}}). \tag{2}$$

Thus, if α is constant before and after the transit time then the slopes of the two regions should add to -2. At room temperature (298 K) for the iridium dendrimer systems studied here, this is not the case. All transients for all generations add up to between -1.2 and -1.4. An example for G1*m*Ir is shown in Fig. 2(b). Deviations from the model have been observed in several systems, including molecularly doped polymers[19] and conjugated polymer systems.[14]

Monte Carlo simulations[19] have shown that the initial decay of the dispersive transient is associated with a certain disorder. The slope of the initial decay for G1*m*Ir (before the transit time) of -0.08 can be compared with simulated transients in Ref. 19 and translates into a Gaussian width of the density of states (DOS), $\hat{\sigma}$ of 4.0. $\hat{\sigma}$ is related to the experimentally accessible σ via Eq. (3)

$$\hat{\sigma}=\frac{\sigma}{kT}. \tag{3}$$

From $\hat{\sigma}$ of 4.0 and $T=298$ K, we obtain an estimate of $\sigma=103$ meV for G1*m*Ir. This is much higher than that measured for structurally well ordered conjugated polymers, where a σ of 52 meV was reported, but comparable to some molecularly doped polymer systems (typically in the region of 80–100 meV)[14] and more disordered conjugated materials, such as PPV.[20]

An important parameter in the understanding of charge transport is the temperature dependence of the mobility and its effect on the shape and the scale of the photocurrent transients. The influence of temperature on the transients is shown in Fig. 3, measured upon a sample of 430 nm thickness. It can be seen from Fig. 3(a) that at high temperatures (343 K), the transit is nondispersive, with a visible plateau region characteristic of Gaussian transport, followed by a broad tail. The transient was measured at a field of 1.2×10^5 V/cm. However at low temperatures (203 K) [Fig. 3(b)], the transient is completely dispersive, since carriers do not attain dynamic equilibrium. The field in this case was 3.25×10^5 V/cm.

A transition from dispersive to nondispersive transport is highly significant and can be interpreted in the framework of earlier simulations based on Monte Carlo methods.[19] These provide a relation that enables calculation of the temperature at which such a transition should occur [Eq. (4)]

$$\hat{\sigma}^2=\left(\frac{\sigma}{kT_c}\right)^2=44.8+6.7\log d, \tag{4}$$

where σ is the width of the DOS, T_c is the transition temperature, and d is the sample thickness in cm. The transition temperature T_c can be obtained from the change in slope of

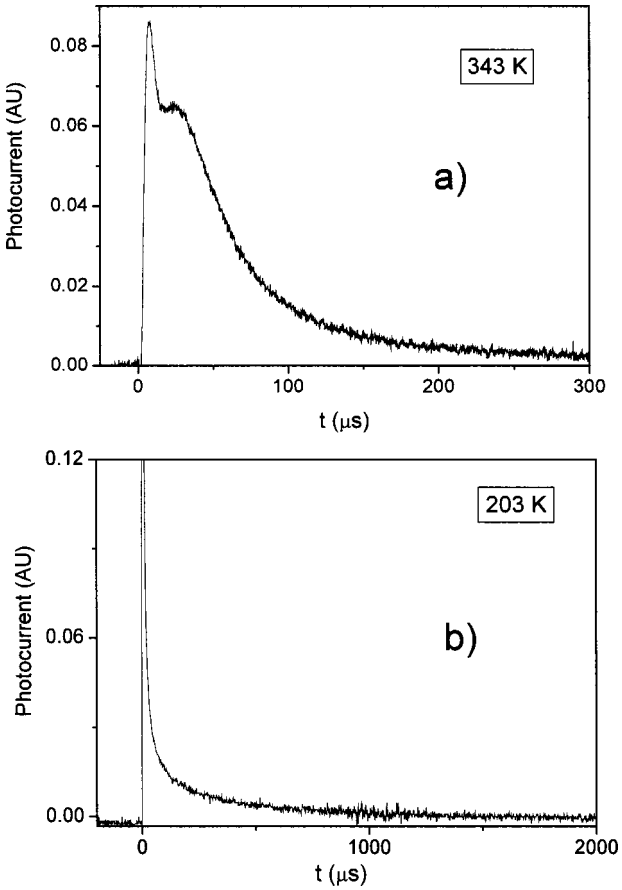

FIG. 3. (a) Transient photocurrent for G1*m*Ir measured at 343 K. (b) G1*m*Ir transient at 203 K.

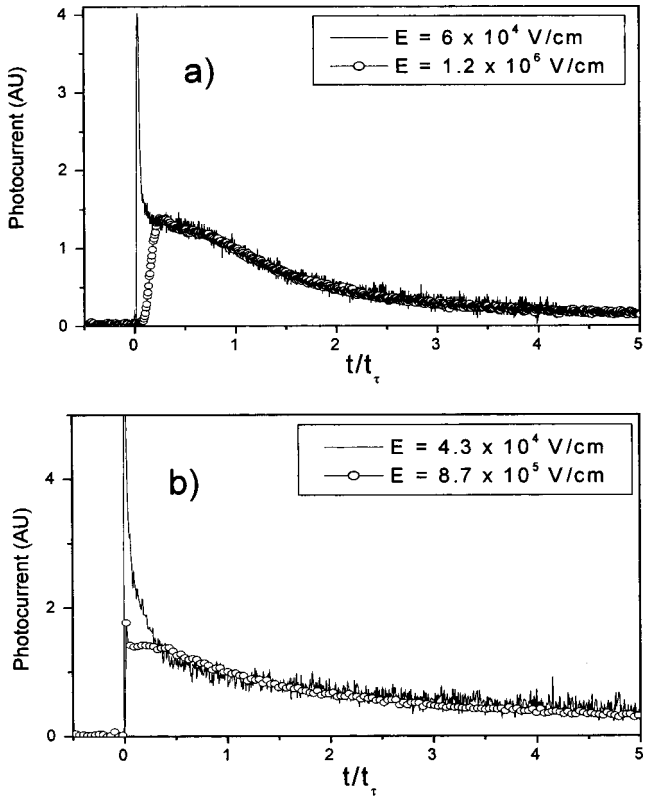

FIG. 5. (a) Room-temperature transient photocurrents of G1*p*Ir at high and low fields normalized to transit time (b) the same for G1*m*Ir.

the graph of the mobility at a given field versus $(1000/T)^2$. Figure 4 shows the temperature dependence of G1*m*Ir at a field of 1.2×10^5 V/cm. The experimentally measured T_c of 293 K is much higher than that reported for a phenyl-amino substituted PPV where a transition temperature of 153 K was measured.[14] For a film thickness of 430 nm and a transition temperature of 293 ± 5 K, this translates to a Gaussian width of DOS of 99.6 ± 1.7 meV.

In Fig. 5(a), transients for G1*m*Ir are shown at two different applied fields, scaled to the transit time. The shapes of the transients are apparently independent of field, even over fields differing by more than an order of magnitude. In the case of Gaussian charge carrier transport, the dispersion of a sheet of carriers migrating through the sample can be calculated from Eq. (5), assuming the validity of the Einstein relation

$$w=\sqrt{\frac{\pi kT}{eU}}, \tag{5}$$

where w is the dispersion, T is the temperature in Kelvin, and U is the applied voltage in V. Using the values for the data in Fig. 2, an applied voltage of 40 V (equivalent to a field of 1.2×10^6 V/cm) and a temperature of 298 K leads to $w=0.045$. Experimentally, the dispersion can be obtained from Eq. (6)

$$w=\frac{t_{1/2}-t_{\mathrm{tr}}}{t_{1/2}}, \tag{6}$$

where t_{tr} is the carrier transit time and $t_{1/2}$ is the time by when the current has decayed to half of the plateau value, From Fig. 2, we obtain $w=0.399$, almost an order of magnitude greater. If the tail broadening of the transients were due to thermal diffusion as expected for Gaussian transport, an increase in field by an order of magnitude would result in a decrease in w by a factor of over 3. This is clearly not seen here. Earlier simulations have shown that the anomalous broadening of tails in TOF signals is a characteristic of non-dispersive transport, due to the Gaussian DOS in these materials.[21] These simulations indicate that the degree of disorder in the material is closely linked with the dispersion.

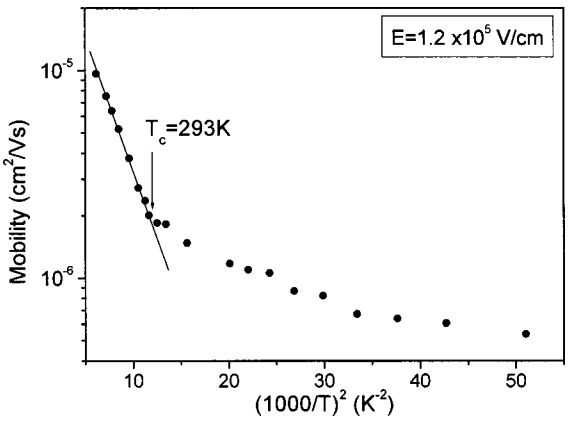

FIG. 4. Mobility vs $(1000/T)^2$ for G1*m*Ir.

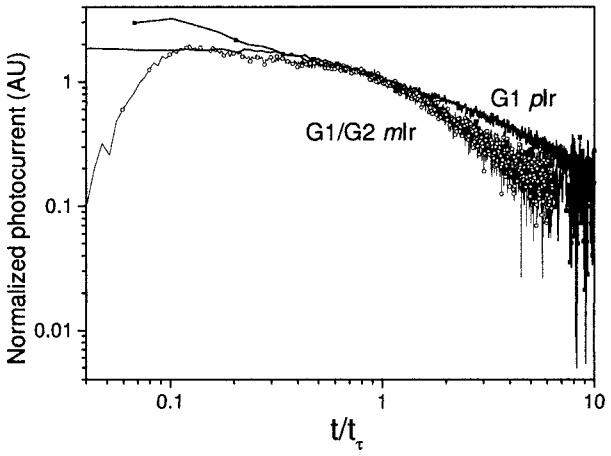

FIG. 6. Transient photocurrents for G1*p*Ir, G1*m*Ir, and G2*m*Ir all scaled by transit time.

The observation of nondispersive transport, albeit at higher temperatures, is in marked contrast to highly disordered materials such as PPV.[22]

We have so far examined the transport properties of a first generation iridium cored phosphorescent dendrimer in detail. We next consider the effect of changing generation, which changes the dendrimer core spacing, and investigate its impact on charge transport. Figure 6 shows traces of G1*m*Ir and G2*m*Ir normalized to the transit time. G1*p*Ir is also shown and will be discussed later. Remarkably, the photocurrent transients are the same for both generations and overlap when scaled by transit time. This shows that the role of the dendrons is to simply slow the carrier packet by separating the core regions, and they have little effect on the tail broadening of the packet. This is a highly significant result that illustrates the power of the dendrimer concept to independently modify material parameters for individual applications. It can be seen from Fig. 5(b) that transients from G1*p*Ir at different fields also scale by transit time, however the tails to these transients are much broader than those seen for G1*m*Ir. This may indicate a greater level of disorder to the transport in this material. This can be seen more clearly when compared to the *meta*-linked dendrimers in Fig. 6.

The electric-field dependence plotted in the Poole–Frenkel formalism[23] of the mobility versus $E^{1/2}$ is shown in Fig. 7(a) for all three dendrimer structures. It can be seen that all three materials give a good fit to this functional form. The generation number and core configuration allow a fine control of the mobility. G1*p*Ir displays a zero-field mobility (μ_0) (calculated by extrapolating the fit to the data to zero field), of 1.9×10^{-6} cm^2/V s. G1*m*Ir has μ_0 a factor of 2 lower at 9.7×10^{-7} cm^2/V s. G2*m*Ir is three times lower still with μ_0 of 3.5×10^{-7} cm^2/V s. However, the field dependence of the three systems is different. Despite having the highest zero-field mobility, the field dependence of G1*p*Ir is much lower than G1*m*Ir, resulting in mobility values that cross at higher fields. G2*m*Ir has a slightly lower field dependence than G1*m*Ir. Yu *et al.*[24,25] have used a geometrical model to explain the origins of field dependence in conjugated materials. Lower field dependence (correlating with an increased value of E_0) is borne of a more rigid geometrical

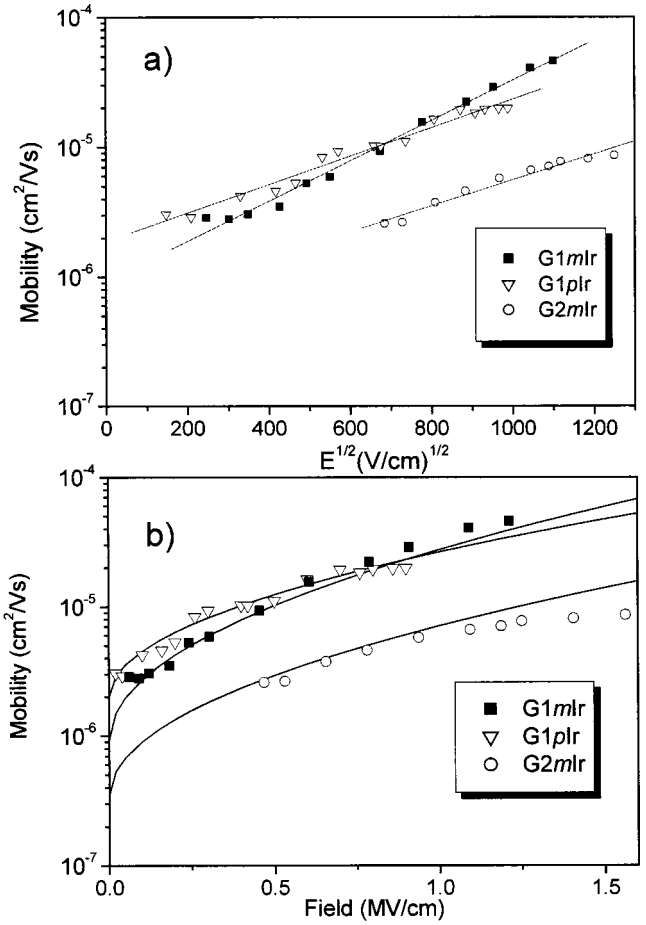

FIG. 7. (a) Poole–Frenkel plot of mobility vs $E^{1/2}$ for all three dendrimer structures. (b) Mobility vs E for all three dendrimer structures. The lines depict fits to $I-V$ data (discussed in Sec. III C).

structure, which allows less perturbation to the morphology under an applied field. The field dependence of the mobility versus E is plotted in Fig. 7(b). The line fits are from a computational model that will be discussed in Sec. III B.

B. Device modeling

As the charge transport measurements using CGL-TOF are made on films of thickness relevant to LEDs, it is instructive to compare those results with measurements of current–voltage ($I-V$) characteristics made on actual devices. Conjugated dendrimers provide excellent systems upon which to study microscopic charge transport properties due to the ability to fine tune the mobility and the independence of morphology on preparation conditions. This can be used to test device models of OLEDs.[26–31] A widely used model has been developed by Davids *et al.*[28] This model is different from the Gaussian disorder model, however, we use it here because it is simpler and still offers useful insight. A combined treatment of thermionic emission over a barrier and tunneling is used to describe the injection of charge into the organic material, which yields the charge-carrier density at the electrode. The coupled Poisson, drift, and continuity equations are then solved through the device using a Poole–Frenkel field dependent mobility of the form shown in Eq. (7)

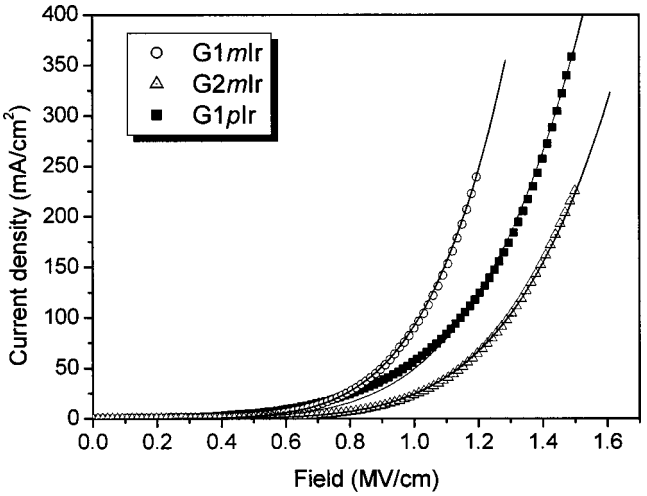

FIG. 8. $I-V$ curves and model fits for G1pIr, G1mIr, and G2mIr hole only devices.

$$\mu_{(E)} = \mu_0 e^{\sqrt{E/E_0}}, \tag{7}$$

where μ_0 and E_0 are the field independent mobility and field dependence of the mobility, respectively. In our implementation, the model is simplified by not accounting for the diffusion of carriers, and we have previously shown good quality fits using this model on both a conjugated polymer[29] and fluorescent conjugated dendrimers.[13] Mobility parameters determined in both of these cases were found to agree with experimental measurements using TOF at room temperature.[27] This model has also been used to calculate the temperature dependence of OLEDs as well as the effect of oxidation on the mobility values.[29] It has been shown previously that injection occurs into the core of the dendrimer[12] and thus the barrier to injection is constant for all generations.

In order to study hole transport in LEDs, we have prepared hole only devices of neat films of each of the three dendrimers with ITO and gold electrodes. A positive voltage was applied to the ITO and the measured current must be due to holes as the barrier to electron injection is around 2.5 eV from the gold electrode. Figure 8 shows the $I-V$ characteristics of 100 nm thick devices. It can be seen that for fields above 0.8 MV/cm, a given current density requires higher fields in the sequence G1mIr, G1pIr, G2mIr. The lines indicate the model fits to the data using the barrier height and the material parameters μ_0 and E_0 as the fitting parameters. The fits to the data qualitatively follow the experimental $I-V$ curves. At lower fields, there are some deviations and this is believed to be due to the influence of space charge on the injection, which is not incorporated into the model.[12]

The mobility parameters obtained by the model for Eq. (7) agree very well with the CGL-TOF data. The fits are shown as the solid lines in Fig. 7(b), and the mobility measured by CGL-TOF as point data. This suggests that the model can provide useful information on charge transport in dendrimer LEDs. The mobility parameters obtained are shown in Table I. The barrier height is essentially similar for all three materials, at ~0.47 eV. ITO is reported to have a work function in the region of 4.8–5.2 eV, depending upon the exact treatment conditions. The highest occupied molecular orbital (HOMO) levels for all three dendrimers have been determined from cyclic voltammetry measurements to be close to 5.6 eV.[32] Hence, the barrier deduced is consistent with plasma treated ITO and the measured dendrimer HOMO.

TABLE I. Fitting parameters for modelling the I–V characteristics of hole only devices.

Material	Barrier height (eV)	μ_0 (cm^2/V s)	E_0 (V/cm)
G1mIr	0.47	9.3×10^{-7}	8.7×10^{4}
G1pIr	0.47	2.0×10^{-6}	1.5×10^{5}
G2mIr	0.48	3.5×10^{-7}	1.1×10^{5}

The EL spectra of the three dendrimers are shown in Fig. 9. Systematic studies of the effect of conjugation on iridium complexes have also shown that substitution onto the pyridine ring affects the position of the lowest unoccupied molecular orbital (LUMO), while the HOMO level has substantial metal character.[33] Thus, one possible explanation as to the origin of the 17 nm redshift for G1pIr may be explained by the lowering of the LUMO level by 0.08 eV, with the HOMO unaffected. The difference in $I-V$ characteristics is then attributable to the morphology of the samples and the effects of the dendron substitution to the core. The values for μ_0 obtained using the model are in very good agreement with those measured by the Poole–Frenkel fits to the CGL-TOF data. The model also correctly shows the reduced field dependence of G1pIr.

C. Controlling device performance by chemical structure

The three materials studied here allow subtle control of charge transport without major changes to the energy levels of the system. We achieve this by use of a single macromolecule and so avoid the potential risk of phase separation that is common in blend systems. Single layer devices were fabricated with 120 nm of neat dendrimer between plasma etched ITO and calcium/aluminum electrodes. The EQEs are

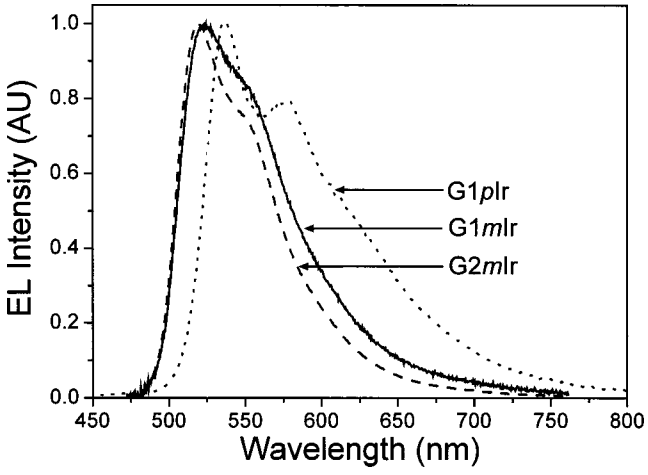

FIG. 9. EL spectra of each of the dendrimers under study.

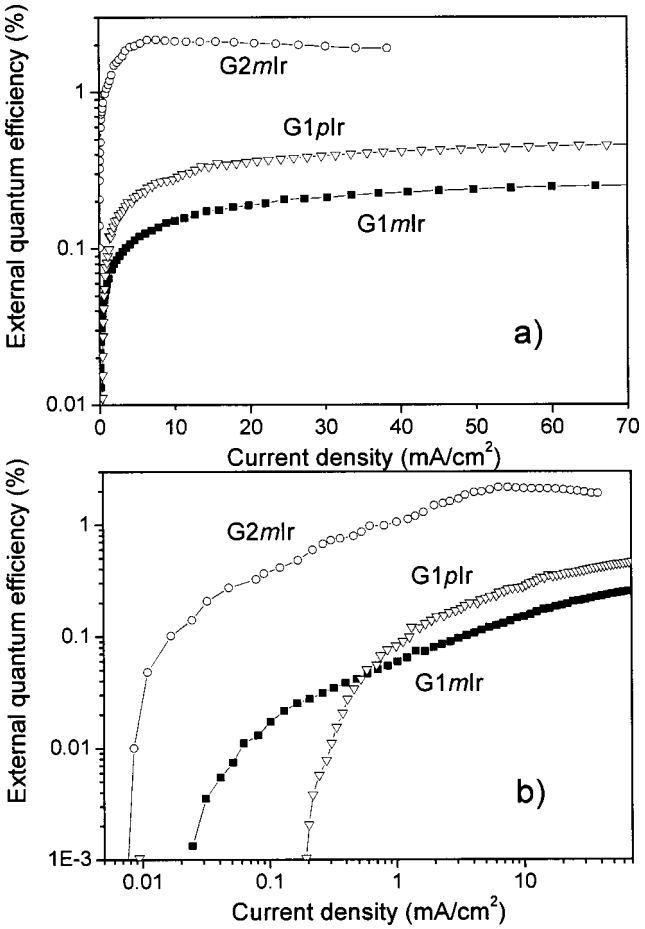

FIG. 10. EQE vs current density for G1*p*Ir, G1*m*Ir, and G2*m*Ir single layer devices with Ca/Al cathodes.

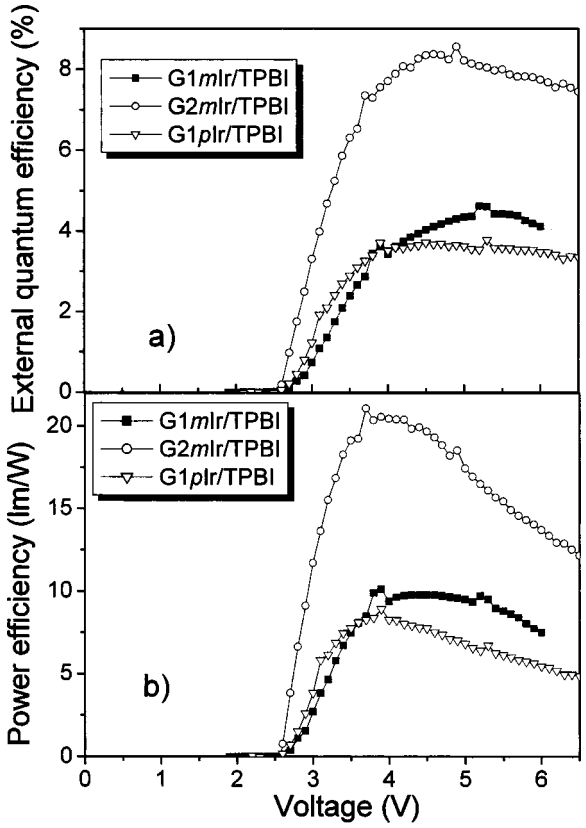

FIG. 11. EQE and power efficiency for dendrimer bilayer devices with TPBI.

shown in Fig. 10, in both semi-logarithmic [Fig. 10(a)] and double logarithmic plots [Fig. 10(b)]. It can be seen that the quantum efficiency of G2*m*Ir is the highest, while G1*m*Ir is greater than G1*p*Ir at low current densities but not at higher ones. It appears, therefore, that for a single layer device, the lower the mobility of the carriers, the higher the quantum efficiency. A single layer device has no confinement mechanism for charge carriers thus it is logical to reason that the lower mobility of holes gives them more opportunity to recombine with electrons before they reach the cathode. This has been shown by Blom and co-workers[34] on a family of PPV derivatives, where the increased quantum efficiency of the lower mobility materials is attributed to a reduction in quenching from the cathode.

It can also be seen from Fig. 10(b) that for both first-generation dendrimers, the EQE does not saturate with current density. This continual increase implies that the charge-carrier balance improves with increasing field. Thus, not only is the effect of increased generation to slow the mobility of the majority carriers, but also to aid carrier balance. This has been observed previously in a family of fluorescent dendrimers, and the increase in efficiency with generation was attributed to the improved balance of carrier transport, allowing relatively mobile holes more opportunity to meet with trapped electrons.[35]

In order to improve the efficiency of OLEDs a heterostructure of hole and electron transporting materials is often used.[1] In addition to the greater charge carrier confinement afforded by such a structure, a build up of charge at the interface between the two materials leads to a feedback mechanism allowing easier injection of carriers into the device. Thus, we fabricated bilayer devices from an 80 nm hole transporting layer of neat dendrimer and 50 nm of electron transporting material, TPBI. A LiF/Al cathode completed the device in this case. The EQEs and power efficiencies of these devices are shown in Fig. 11. Again, it can be seen that the dendrimer generation has a large effect on the performance of these devices. G2*m*Ir shows double the EQE and power efficiency of the G1 devices. However, in this instance, the difference between the two first generation dendrimers is smaller. Excellent power efficiencies of 20 lm/W for neat G2*m*Ir-based bilayers and 10 lm/W for neat G1*m*Ir-based devices render these high efficiencies for solution processed OLEDs with neat emissive layers. This shows that the ability to fine tune the charge transport by dendrimer generation and structure is a useful tool for making balanced and efficient devices.

IV. CONCLUSION

We have reported a detailed study of charge transport in electrophosphorescent organic semiconductors. The materials studied here are dendrimers closely related to *fac*-tris(2-phenylpyridyl) iridium (III) [$Ir(ppy)_3$] which is widely used in OLEDs. We find that we can fine tune the mobility by

dendrimer generation, and that the transport dynamics can be related to the structural configuration of the dendrimers. In addition, we have investigated both the field and the temperature dependence of these unique materials. The TOF indicates that energetic disorder can account for the general transport properties in these materials. A σ of 100 meV corresponds well with that measured for some molecularly doped polymers and some of the more disordered conjugated polymers. The transport is weakly dispersive at room temperature, and a transition to nondispersive transport is seen at elevated temperatures. A measured transition temperature T_c of 293 K is much higher than that measured for conjugated polymers. This may be due to specific properties of the metal complex core or disorder introduced by the morphological properties of the dendrimer. We show that by increasing the generation of the dendrimer, we simply lower the mobility and do not increase the level of disorder in the film, as reflected in identical levels of tail broadening for the first- and second-generation material. By increasing the generation, we are able to improve the balance of charge carriers and are able to create efficient single layer LEDs. In addition, even higher efficiencies can be obtained in a bilayer structure, with the dendrimer architecture having a large impact on the performance of the device.

ACKNOWLEDGMENTS

The authors thank Dr. J. M. Lupton for supplying the charge transport model and for helpful advice. They are very grateful to Professor K. Müllen for providing the perylene derivative. The authors acknowledge financial support from EPSRC, SHEFC, CDT Oxford Ltd, the EU project LAMINATE, the Optodynamics Centre of the Phillips University in Marburg, and the Fond der Chemischen Industrie. One of the authors (I. D. W. S.) is a Royal Society University Research Fellow.

[1] C. W. Tang and S. A. Van Slyke, Appl. Phys. Lett. **51**, 913 (1987).
[2] J. H. Burroughes, D. D. C. Bradley, A. R. Brown, R. N. Marks, K. Mackay, R. H. Friend, P. L. Burn, and A. B. Holmes, Nature (London) **347**, 539 (1990).
[3] M. Halim, J. N. G. Pillow, I. D. W. Samuel, and P. L. Burn, Adv. Mater. (Weinheim, Ger.) **11**, 371 (1999).
[4] P. W. Wang, Y. J. Liu, C. Devadoss, P. Bharathi, and J. S. Moore, Adv. Mater. (Weinheim, Ger.) **8**, 237 (1996).
[5] M. Ikai, S. Tokito, Y. Sakamoto, T. Suzuki, and Y. Taga, Appl. Phys. Lett. **79**, 156 (2001).
[6] C. W. Tang, Inf. Disp. **12**, 16 (1996).
[7] M. A. Baldo, D. F. O'Brien, Y. You, A. Shoustikov, S. Sibley, M. E. Thompson, and S. R. Forrest, Nature (London) **395**, 151 (1998).
[8] M. A. Baldo, S. Lamansky, P. E. Burrows, M. E. Thompson, and S. R. Forrest, Appl. Phys. Lett. **75**, 4 (1999).
[9] C.-L. Lee, K. B. Lee, and J-J. Kim, Appl. Phys. Lett. **77**, 2280 (2000).
[10] J. P. J. Markham, S.-C. Lo, S. W. Magennis, P. L. Burn, and I. D. W. Samuel, Appl. Phys. Lett. **18**, 13 (2002).
[11] S.-C. Lo, N. A. H. Male, J. P. J. Markham, S. W. Magennis, P. L. Burn, O. V. Salata, and I. D. W. Samuel, Adv. Mater. (Weinheim, Ger.) **13**, 975 (2002).
[12] J. P. J. Markham, T. D. Anthopoulos, I. D. W. Samuel, G. J. Richards, P. L. Burn, C. Im, and H. Bässler, Appl. Phys. Lett. **81**, 3266 (2002).
[13] J. M. Lupton, I. D. W. Samuel, R. Beavington, M. J. Frampton, P. L. Burn, and H. Bässler, Phys. Rev. B **63**, 155206 (2001).
[14] D. Hertel, H. Bässler, U. Scherf, and H. H. Hörhold, J. Chem. Phys. **110**, 9214 (1999).
[15] H. C. F. Martens, P. W. M. Blom, and H. F. M. Schoo, Phys. Rev. B **61**, 7489 (2000).
[16] R. J. O. M. Hoofman, M. P. de Haas, L. D. A. Siebbeles, and J. M. Warman, Nature (London) **392**, 54 (1998).
[17] N. C. Greenham, R. H. Friend, and D. D. C. Bradley, Adv. Mater. (Weinheim, Ger.) **6**, 491 (1994).
[18] H. Scher and E. W. Montroll, Phys. Rev. B **12**, 2455 (1975).
[19] P. M. Borsenberger, L. T. Pautmeier, and H. Bässler, Phys. Rev. B **46**, 12145 (1992).
[20] E. Lebedev, T. Dittrich, V. Petrova-Koch, S. Karg, and W. Brütting, Appl. Phys. Lett. **71**, 2686 (1997).
[21] P. M. Borsenberger and H. Baessler, J. Appl. Phys. **75**, 967 (1994).
[22] P. W. M. Blom and M. C. J. M. Vissenberg, Phys. Rev. Lett. **80**, 3819 (1998).
[23] H. Bässler, Phys. Status Solidi B **15**, 175 (1993).
[24] Z. G. Yu, D. L. Smith, A. Saxena, R. L. Martin, and A. R. Bishop, Phys. Rev. Lett. **84**, 721 (2000).
[25] Z. G. Yu, D. L. Smith, A. Saxena, R. L. Martin, and A. R. Bishop, Phys. Rev. B **63**, 085202 (2001).
[26] B. K. Crone, I. H. Campbell, P. S. Davids, D. L. Smith, C. J. Neef, and J. P. Ferraris, J. Appl. Phys. **86**, 5767 (1999).
[27] I. H. Campbell, D. L. Smith, C. J. Neef, and J. P. Ferraris, Appl. Phys. Lett. **74**, 2809 (1999).
[28] P. S. Davids, I. H. Campbell, and D. L. Smith, J. Appl. Phys. **82**, 6319 (1997).
[29] J. M. Lupton and I. D. W. Samuel, J. Phys. D **32**, 2973 (1999).
[30] I. H. Campbell, P. S. Davids, D. L. Smith, N. N. Barashkov, and J. P. Ferraris, Appl. Phys. Lett. **72**, 1863 (1998).
[31] I. H. Campbell, D. L. Smith, C. J. Neef, and J. P. Ferraris, Appl. Phys. Lett. **75**, 841 (1999).
[32] S.-C. Lo, E. B. Namdas, P. L. Burn, and I. D. W. Samuel, Macromolecules (to be published).
[33] S. Lamansky, P. Djurovich, D. Murphy, F. Abdel-Razzaq, H-E. Lee, C. Adachi, P. E. Burrows, S. R. Forrest, and M. E. Thompson, J. Am. Chem. Soc. **123**, 4304 (2001).
[34] P. W. M. Blom, M. C. J. M. Vissenberg, J. N. Huiberts, H. C. F. Martens, and H. F. M. Schoo, Appl. Phys. Lett. **77**, 2057 (2000).
[35] J. M. Lupton, I. D. W. Samuel, R. Beavington, P. L. Burn, and H. Bässler, Adv. Mater. (Weinheim, Ger.) **13**, 258 (2001).